Particle Sizing using Passive Ultrasonic Measurement of Particle-Wall Impact Vibrations

G. Carson[†,*], A. J. Mulholland[†], A. Nordon[‡], M. Tramontana[⋆], A. Gachagan[⋆] and G. Hayward[⋆]

[†] Department of Mathematics, University of Strathclyde, Glasgow, UK, G1 1XH.

[‡] WestCHEM, Department of Pure and Applied Chemistry and Centre for Process Analytics and Control Technology (CPACT), University of Strathclyde, 295 Cathedral Street, Glasgow, UK, G1 1XL.

[⋆] Department of Electronic and Electrical Engineering, The Centre for Ultrasonic Engineering (CUE), University of Strathclyde, Royal College Building, 204 George Street, Glasgow, UK, G1 1XW.

February 26, 2008

[*]corresponding author: Department of Mathematics, University of Strathclyde, Livingstone Tower, 26 Richmond Street, Glasgow G1 1XH, U.K., Tel: ++44 (0)141 548 3286, Fax: ++44 (0)141 548 3345, email: rs.gcar@maths.strath.ac.uk

Abstract

In continuously stirred reactor vessels the non-invasive recovery of the particle size could be used to monitor the reaction process. Experimental and numerical investigations have shown empirically that the frequency of the peak vibration response arising from the particle-wall impact is inversely proportional to the particle size. The passive monitoring of these impact vibrations using an ultrasonic transducer has the potential therefore of non-invasively recovering the particle size. However, the vessel geometry, fluid loading, variable impact position and velocity, stirrer and transducer effects, and noise levels make this problem very complex. There are a large number of system parameters and this makes empirical derivations of cause and effects extremely difficult. The first objective of this paper is to derive an analytical expression for the vibrations arising from a spherical particle impacting a circular plate. Using a series expansion in terms of the plate loss parameter, an expression for the frequency of the peak pressure in terms of the system parameters is derived. In particular, its explicit dependency on the impacting particle size and the impact velocity is found. The inverse problem of recovering the particle size from the experimental data is then investigated. A set of experiments are described where the impact vibrations are recorded using an ultrasonic transducer attached to the rear of a thin plate. The results show that it is possible to recover the particle size using this approach. Data from a second set of experiments, involving multi-particle impact with a vessel wall in a continuously stirred reactor, are then used. The inverse problem of recovering the particle size from the vibration spectrum was then investigated with encouraging results.

1 Introduction

The use of ultrasonics as a process measurement technique has many advantages which are due in part to it being non-invasive and relatively inexpensive [1]. In batch reactors, containing a particle laden fluid, the recovery of the particle size could be used to monitor the reaction process. Controlled experiments have shown that time domain vibrations arising from single particles colliding with a plate can be used to recover the size of the impacting particle [2, 3]. However, this approach depends on identifying the contact duration and this is not practical in multi-particle plate interactions such as in a stirred, particle laden fluid in a reactor vessel [4]. This problem can be circumvented by analysing the signal in the frequency domain. Both single particle [5] and multi-particle [6] interactions with a plate have been studied in this way. Here the radiated sound wave was measured using a microphone. These investigations have relied on either experimental evidence or by solving the governing equations numerically and, by running many simulations, making empirical observations regarding the dependency of key features in the frequency response on the system parameters. In particular it was found that the frequency of the peak pressure was inversely proportional to the particle size (see [4] and references therein). There is motivation therefore to interrogate a mathematical model of this particle-plate interaction to explicitly show this dependency. Such an investigation will also be able to comment on the dependency of the frequency response on other system parameters and its relative sensitivity to changes in these parameters. The first objective of this paper is to derive analytically an expression for the frequency of the peak response that shows explicitly its dependency on the system parameters, in particular the particle size.

The multi-particle impact experiments described in [4] involve a particle laden fluid being continuously stirred in a bell shaped reactor vessel. The vessel geometry, fluid loading, variable impact position and velocity, stirrer and transducer effects, and noise levels make this problem very complex. There are a large number of system parameters and this makes empirical derivations of cause and effects extremely difficult. To help establish the relationships that have been found between the spectral vibration response

and the system parameters, theoretical modelling can be used. A first step in this analysis is to examine a simpler, and more controlled, experimental set-up. To this end, this paper will start with a well-established model for the impact of a spherical particle with a thin circular plate [7] and show, using a set of approximations based on series expansions, the explicit dependency of the peak pressure frequency on the system parameters. To validate this approach an experiment involving spherical particles being dropped onto a circular plate is utilised. In contrast to previous work the vibration response of the plate is measured using an ultrasonic transducer in contact with the plate. The experiments will show that the peak pressure does decrease as the particle size increases; in agreement with the experimental observations in [6] and [4].

One motivation for developing our understanding of these complex interactions is to help in the development of a non-invasive technique that can recover information about the system parameters such as the particle size [8, 9, 10, 11, 12, 13, 14, 15, 16]. The second objective of this paper is therefore to construct an inverse methodology, that utilises the data from single particle experiments and the above model, to automatically recover the particle size. Encouraged by these results, some multi-particle experimental data is then used to recover the particle size in this setting. Remarkably, it transpires that the method can still recover the particle size even though many of the additional complexities of these experiments are neglected in this initial model. This paper therefore derives for the first time the explicit dependency of the frequency of the peak pressure on the system parameters and, from the knowledge gained, develops a method for automating the recovery of the particle size from impact vibration spectra obtained using an ultrasonic transducer.

2 Analytical approximation of the acoustic emission spectrum

In order to make analytical headway the situation of a single particle being dropped onto a thin circular plate is considered in this section. Therefore the added complications of

the vessel geometry and fluid loading effects are neglected. The validation of the model will also be simplified as the experiments can be conducted in a more controlled fashion. This will allow us to comment upon the sensitivity of the spectral response to particle size, impact velocity, and impact position. In the following, an asymptotic expansion in the plate loss factor and a Taylor series expansion in the frequency domain will lead to an analytical expression for the particle-plate vibration spectrum. This then facilitates a discussion on the dependency of the acoustic emission spectrum on the system parameters and in particular the particle size. The classical equation for the motion of a damped plate, subject to an excitation due to an impacting particle, can be solved to give an expression for the displacement of the plate [7]. A relatively large thin plate is considered so that the amplitude of the flexural vibrations dominates; the frequency of interest will also be well removed from the frequency of the main longitudinal harmonics in the thickness direction. The particles will be dropped onto the centre of the circular plate and so attention is restricted to the axisymmetric flexural vibrations of a homogeneous circular plate. The particles and the plate are made from glass and it is therefore assumed that the collision is elastic, with no permanent deformations remaining after the impact. By assuming that the particle-plate contact time is less than the time taken for a wave to reflect off the plate extremities and return to the impact location, the Hertz contact theory coupled with Zener's treatment of a non-rigid plate of finite thickness gives the plate displacement as [17]

$$
\begin{aligned}
u(r,t) &= \frac{F_0}{M}\sum_{n=1}^{\infty}\frac{\phi_n(0)\phi_n(r)}{(4\omega_0^2-\omega_n^2)\sin(e_1)-2\eta\omega_n\omega_0\cos(e_1)} \qquad (1)\\
\times &\begin{cases}
\frac{1}{2}\sin(2\omega_0 t+e_1)+e_5\,e^{-\frac{\eta\omega_n t}{2}}\sin(\omega^* t+e_4)+e_3, \\
\qquad\qquad\qquad\qquad\qquad \text{if } 0\le t\le\frac{\pi}{\omega_0}, \\
\\
e_9\,e^{-\frac{\eta\omega_n t}{2}}\sin(\omega^* t+e_8), \qquad \text{if } t>\frac{\pi}{\omega_0},
\end{cases}
\end{aligned}
$$

where

$$
\begin{aligned}
e_1 &= \tan^{-1}(\frac{1}{e_2\eta}),\ e_2=\frac{2\omega_0\omega_n}{\omega_n^2-4\omega_0^2}, \qquad (2)\\
e_3 &= \frac{(4\omega_0^2-\omega_n^2)\sin(e_1)-2\eta\omega_0\omega_n\cos(e_1)}{2\omega_n^2}, \qquad (3)
\end{aligned}
$$

$$e_4 = \tan^{-1}\left(\frac{2\omega_0}{(e_2\omega_n + \omega_0)\eta}\right), \tag{4}$$

$$e_5 = \frac{\omega_0 \cos(e_1)}{\frac{\eta}{2}\omega_n \sin(e_4) - \omega^* \cos(e_4)}, \tag{5}$$

$$e_6 = \frac{1}{2}\sin(e_1) + e_5\, e^{-\frac{\eta\omega_n\pi}{2\omega_0}} \sin\left(\frac{\omega^*\pi}{\omega_0} + e_4\right) + e_3, \tag{6}$$

$$e_7 = \omega_0 \cos(e_1) + e_5\, e^{-\frac{\eta\omega_n\pi}{2\omega_0}} \left(\omega^* \cos\left(\frac{\omega^*\pi}{\omega_0} + e_4\right)\right.$$

$$\left. - \frac{\eta}{2}\omega_n \sin\left(\frac{\omega^*\pi}{\omega_0} + e_4\right)\right), \tag{7}$$

$$e_8 = \tan^{-1}\left(\frac{e_6\omega^*}{e_7 + \frac{\eta}{2}e_6\omega^*}\right), \tag{8}$$

$$e_9 = \frac{e_7}{\omega^* \cos(e_8) - \frac{\eta}{2}\omega_n \sin(e_8)}, \tag{9}$$

$$M = \rho\pi a^2 h, \tag{10}$$

$$\omega^* = \omega_n\sqrt{1-\eta^2}, \tag{11}$$

η is the internal loss factor, F_0 is the impact force amplitude, M is the mass of the plate, ω_n are the natural plate frequencies, ω_0 is the frequency of vibration associated with the particle-plate contact duration, ρ is the plate density, a is the plate radius, h is the plate thickness, r is the distance from the particle impact point to the centre of the plate, ϕ_n are the eigenfunctions of the plate given by,

$$\phi_n(r) = \frac{1}{\sqrt{2}}\left(\frac{J_0(\frac{\lambda_n r}{a})}{J_0(\lambda_n)} - \frac{I_0(\frac{\lambda_n r}{a})}{I_0(\lambda_n)}\right). \tag{12}$$

and the eigenvalues λ_n are given by the solution to

$$J_0(\lambda_n)I_1(\lambda_n) + J_1(\lambda_n)I_0(\lambda_n) = 0. \tag{13}$$

Figure 5 shows a typical plot of Equation (1) where the dotted line shows the point, $t = \pi/\omega_0$, at which the first branch ends and the second begins. After the impact, the plate undergoes a very rapid displacement. Its recovery to the equilibrium occurs over a far larger time scale and is oscillatory in nature. The second branch of Equation (1) is therefore dominant and the associated power spectrum, obtained by a numerical Fast Fourier Transform, shows that neglecting the first branch in the solution does not result in any significant change in the spectrum. The analysis can therefore be simplified by concentrating solely on the second branch of Equation (1). Each of the components in

Equation (1) is now expanded as an asymptotic series in the loss parameter $\eta \ll 1$. Expanding Equation (2) gives

$$e_1 = -\frac{\pi}{2} - e_2\eta + O(\eta^3), \tag{14}$$

and so $\sin(e_1) = -1 + O(\eta^2)$, $\cos(e_1) = -e_2\eta + O(\eta^3)$ and therefore Equation (3) becomes

$$e_3 = \frac{1}{2} - \frac{2\omega_0^2}{\omega_n} + O(\eta^2). \tag{15}$$

From Equation (11), $\omega^* = \omega_n + O(\eta^2)$, and hence in Equation (4)

$$e_4 = -\frac{\pi}{2} - b_1\eta + O(\eta^3), \tag{16}$$

where $b_1 = 1/2 + \omega_n^2/(\omega_n^2 - 4\omega_0^2)$. Equation (5) is then given by

$$e_5 = -\frac{2\omega_0^2}{\omega_n^2} + O(\eta^2). \tag{17}$$

Equation (6) can be written as

$$e_6 = \frac{2\omega_0^2(e^{-\frac{\eta\omega_n\pi}{2\omega_0}}\cos(\frac{\pi\omega_n}{\omega_0} - \eta(\frac{1}{2} + \frac{\omega_n^2}{\omega_n^2 - 4\omega_0^2})) - 1)}{\omega_n^2}, \tag{18}$$

and hence

$$e_6 = \hat{f}_1 + \hat{f}_2\eta + O(\eta^2), \tag{19}$$

where

$$\hat{f}_1 = \frac{2\omega_0^2(\cos(\frac{\pi\omega_n}{\omega_0}) - 1)}{\omega_n^2},$$

and

$$\hat{f}_2 = \omega_0\left(\frac{\omega_0(3\omega_n^2 - 4\omega_0^2)\sin[\frac{\pi\omega_n}{\omega_0}]}{\omega_n^4 - 4\omega_n^2\omega_0^2} - \frac{\pi\cos[\frac{\pi\omega_n}{\omega_n}]}{\omega_n}\right).$$

Treating Equation (7) in a similar way

$$e_7 = \omega_0\hat{f}_3 + \omega_0\hat{f}_4\eta + O(\eta^2), \tag{20}$$

where

$$\hat{f}_3 = -\frac{2\omega_0\sin(\frac{\pi\omega_n}{\omega_0})}{\omega_n},$$

and

$$\hat{f}_4 = \frac{2\omega_n\omega_0\cos(\frac{\pi\omega_n}{\omega_0}) + \pi(\omega_n^2 - 4\omega_0^2)\sin(\frac{\pi\omega_n}{\omega_0}) - 2\omega_n\omega_0}{\omega_n^2 - 4\omega_0^2}.$$

Now substituting Equations (19) and (20) into Equation (8) gives

$$e_8 = \hat{f}_5 + \hat{f}_6\eta + O(\eta^2), \tag{21}$$

where $\hat{f}_5 = \tan^{-1}(\omega_n\hat{f}_1/\omega_0\hat{f}_3)$ and $\hat{f}_6 = -\omega_n(\omega_n\hat{f}_1{}^2 + 2\omega_0\hat{f}_4\hat{f}_1 - 2\omega_0\hat{f}_2\hat{f}_3)/2(\omega_0^2\hat{f}_3{}^2 + \omega_n^2\hat{f}_1{}^2)$. Hence Equation (9) becomes

$$e_9 = \hat{f}_7 + \hat{f}_8\eta + O(\eta^2), \tag{22}$$

where $\hat{f}_7 = \omega_0\hat{f}_3\sec(\hat{f}_5)/\omega_n$ and $\hat{f}_8 = \omega_0\sec(\hat{f}_5)(2\hat{f}_4 + \hat{f}_3(1 + 2\hat{f}_6)\tan(\hat{f}_5))/2\omega_n$. From Equation (22)

$$\hat{f}_7 \approx \hat{f}_8\eta,$$

which implies that $\hat{f}_8 \gg \hat{f}_7$ as $\eta \ll 1$. So $e^{(-\eta\omega_n t/2)} \approx f_7 + f_8\eta$ in the second branch of Equation (1) and, by letting $\psi = \omega_n/\omega_0$, this can be rewritten to give the plate displacement as

$$\begin{aligned} u(r,t) &= \frac{F_0}{M}\sum_{n=1}^{\infty}\phi_n(r)\phi_n(0) \\ &\times \frac{1}{\omega_n^2 - 4\omega_0^2}((f_7 + f_8\eta)\sin(\omega_n t + f_5) \\ &+ (f_7 f_6\eta)\cos(\omega_n t + f_5)) + O(\eta^2), \end{aligned} \tag{23}$$

where

$$\begin{aligned} f_1 &= \frac{2(\cos(\psi\pi) - 1)}{\psi^2}, \\ f_2 &= \frac{(3\psi^2 - 4)\sin(\psi\pi) - \pi(\pi^2 - 4)\cos(\psi\pi)}{\psi^2(\psi^2 - 4)}, \\ f_3 &= -\frac{2\sin(\psi\pi)}{\psi}, \\ f_4 &= \frac{2\psi(\cos(\psi\pi) - 1)}{\psi^2 - 4} + \pi\sin(\psi\pi), \\ f_5 &= \frac{\psi\pi}{2}, \\ f_6 &= \frac{4 - 3\psi^2}{2(\psi^2 - 4)} + \frac{\pi}{4}(\cot(f_5) + (\psi - 1)\sin(\psi\pi)), \\ f_7 &= -\frac{4}{\psi^2}\sin(f_5), \\ \text{and} \qquad f_8 &= \frac{\pi}{\psi^2}(\psi + (\psi - 1)\cos(\psi\pi))\sin(f_5). \end{aligned}$$

This approximate solution (23) for the plate displacement is compared with Equation (1), in Figure 5. Since the transducer detects the force at impact, the acceleration is plotted, and it can be seen that reasonable agreement is achieved. Note that, in this paper, we are solely concerned with frequency shifts in the peak response and not in the magnitude of the peak response. The ultrasonic transducer used in the experiment converts the impact force to a voltage and so colours the spectrum with its own transfer function. The model presented here does not take account of this conversion nor the effect that the transducer response has on the spectrum. In addition, when we use the model to recover the particle size, as detailed in the next section, the spectral data is integrated and normalised. As such the magnitude is expressed in arbitrary units in Figure 5. The advantage of this approximation is that an analytic expression for the frequency domain spectrum can been derived. Differentiating twice with respect to time, an expression for the plate acceleration is given by

$$\ddot{u}(r,t) = \frac{F_0}{M}\sum_{n=1}^{\infty}\frac{\phi_n(0)\phi_n(r)}{\omega_n^2 - 4\omega_0^2}(-\eta f_6 f_7 \omega_n^2 \cos(\omega_n t + f_5) - (\eta f_8 + f_7)\omega_n^2 \sin(\omega_n t + f_5)), \quad (24)$$

and, by combining the trigonometric terms, Equation (24) can be viewed as a Fourier cosine series

$$\ddot{u}(r,t) = \sum_{n=1}^{\infty} A_n \cos(\omega_n t + \theta_1), \quad (25)$$

where

$$\begin{aligned} A_n &= (F_0\phi_n(0)\phi_n(r))/M(\omega_n^2 - 4\omega_0^2)\sqrt{X_2^2 + Y_2^2}, \\ \theta_1 &= \tan^{-1}\frac{Y_2}{X_2}, \\ X_2 &= -\omega_n^2(\eta f_6 f_7 \cos(f_5) + (\eta f_8 + f_7)\sin(f_5)), \\ Y_2 &= \omega_n^2(\eta f_6 f_7 \sin(f_5) - (\eta f_8 + f_7)\sin(f_5)). \end{aligned}$$

It is found that the amplitude of the harmonics A_n decreases as n increases (due to the increase in ω_n in the denominator) and so we can approximate the acceleration by restricting attention to a finite number of terms in the summation. In addition, if the impact location r is small compared to the plate radius a then, for small values of $\lambda_n r/a$, we can approximate $\phi_n(r)$ in Equation (12) by $\phi_n(0)$. The dependency of the spectrum

on the impact location is thus removed from the model. Numerical simulations of the original model given by Equation (1) show that the frequency of the peak response is dominated by changes in the particle size, with the impact location having a far lesser effect. The experiments discussed in the sections that follow also support this assumption that the shift in the frequency response is less sensitive to variations in the impact location than to variations in the particle size. It can then be shown that $\phi_n(0)^2 \approx \pi^2 n/2$ [18]. The peak force of impact F_0 and the mass of the plate M only affect the magnitude of the spectrum and not the shape of its frequency profile. Hence we can concentrate on a scaled acceleration amplitude $\hat{a}_n = A_n M/F_0$. Treating ω_n as a continuous variable allows a Taylor series expansion about the point ω_0 to give

$$\begin{aligned}
\hat{a}_n &= \frac{-\sqrt{P_0}}{9} - \frac{288 - 144\eta\pi + \eta^2(27\pi^2 - 56)}{27\sqrt{P_0}\omega_0}(\omega - \omega_0) \\
&+ \frac{1}{3P_0^{3/2}\omega_0^2}(96(9\pi^2 - 56) - 96\eta\pi(9\pi^2 - 56) + 3\eta^3\pi(192 + 40\pi^2 - 9\pi^4) \\
&+ \eta^4(48 - 82\pi^2 + 64\pi^4) + 18\eta^2(-64 - 88\pi^2 + 15\pi^4)(\omega - \omega_0)^2 \\
&+ O((\omega - \omega_0)^3), \qquad (26)
\end{aligned}$$

where $P_0 = 144 - 72\eta\pi + \eta^2(9\pi^2 + 4)$. The location of the first maximum, ω_{max}, is then approximately

$$\omega_{max} = P_1(\eta)\omega_0, \qquad (27)$$

where

$$\begin{aligned}
P_1(\eta) &= (1728(9\pi^2 - 32) - 1728\eta\pi(9\pi^2 - 32) - 54\eta^3\pi(9\pi^4 + 20\pi^2 - 256) \\
&+ 108\eta^2(45\pi^4 - 108\pi^2 - 256) + \eta^4(351\pi^4 - 1872\pi^2 + 640)) \\
&/ (18(96\eta\pi(56 - 9\pi^2) + 96(9\pi^2 - 56) + 3\eta^3\pi(192 + 4\pi^2 - 4\pi^4) \\
&+ \eta^4(6\pi^4 - 82\pi^2 + 48) + 18\eta^2(15\pi^4 - 88\pi^2 - 64))). \qquad (28)
\end{aligned}$$

That is, the location of the first peak in the impact spectrum is directly proportional to ω_0 (as empirically derived in [2, 3]). Now $\omega_0 = \pi/T_h$, where T_h is the contact duration time [7]

$$T_h = \frac{4}{5}\sqrt{\pi}\frac{\Gamma(2/5)}{\Gamma(9/10)}\frac{\alpha_m}{u_0},$$

where $\alpha_m = (5u_0^2 m/4k)^{2/5}$, $k = 4\sqrt{b}/3z$, $z = (1-\nu_{pl}^2)/E_{pl} + (1-\nu_b^2)/E_b$, where E_b, E_{pl}, ν_b and ν_{pl} are the Young's Moduli and Poisson's Ratio of the particle and plate materials respectively. Hence

$$\omega_{max} = \frac{5\sqrt{\pi}\Gamma(9/10)P_1}{4\Gamma(2/5)}\left(\frac{4}{5\pi}\right)^{2/5}\frac{u_0^{1/5}}{b(\rho_b z)^{2/5}}. \tag{29}$$

The dependency of P_1 on the damping coefficient is shown in Figure 5. Although there is a steep gradient for $0.4 < \eta < 0.6$, the actual value for the damping coefficient is always much lower. In the next section, a simplified experiment is described wherein a particle is dropped onto a glass plate from a height H and since $u_0 = \sqrt{2gH}$, where g is the gravitational constant, then

$$\omega_{max} = \frac{5\sqrt{\pi}\Gamma(9/10)P_1}{2\Gamma(2/5)}\left(\frac{4}{5\pi}\right)^{2/5}\frac{(gH)^{1/10}}{b(\rho_b z)^{2/5}}. \tag{30}$$

Thus, as the particle size increases, the first peak in the vibration spectrum, ω_{max}, will move to a lower frequency. In a similar way, as the particle density increases, ω_{max} will shift to a lower frequency, and as the particle velocity is increased (i.e. H is increased), ω_{max} will move to a higher frequency. As can be seen from Equation (30) the frequency shift in the spectrum is not very sensitive to the height that the particle is dropped from (the impact velocity). This result is in agreement with the experimental findings detailed in the sections that follow. Figure 5 shows the main lobe of the model spectrum shifting to the lower end of the frequency domain as the particle size is increased, as predicted by Equation (30).

3 Inverse Problem I: Recovery of the particle size from single-particle experiments

To test the model a set of experiments examined the simplified case of a single particle being dropped onto a glass plate; full details of these experiments are detailed elsewhere [19]. The time domain vibrations of the plate were captured using an ultrasonic transducer attached to the rear of the plate. A high sampling rate (2 MHz) was used, together with a

pre-amplifier and some basic signal processing using low and high-pass filters. In this controlled environment the background noise levels were low and all other significant sources of vibration (such as the rotation of the stirrer in the batch reactor experiments) were removed. This ensured that the highly transient impact of this single particle and the resulting plate vibration could be very clearly seen in the time domain plots. The time frame containing the impact vibration and resulting vibrations is then extracted and converted to the frequency domain using a Fast Fourier Transform. Experiments were performed using glass beads with size categories of $400-500\mu$m, $500-600\mu$m and $850-1000\mu$m. The beads were repeatedly dropped from different measured heights onto the centre of a glass plate on top of a Nano 30 piezoelectric transducer [20], and the response recorded. Although the magnitude changes, it was found that the form of the resulting spectral response was relatively insensitive to variations in this height. The impact location was also varied and again, although the amplitude of the spectrum is affected, the frequency of the peak response was relatively insensitive to these changes. Note that this paper focuses on the theoretical development of the particle-plate impact model and its comparison with experimental findings. As such, the full experimental detail is omitted and can be found elsewhere [19]. To quantitatively compare the model with the experiment and to facilitate the recovery of the particle size using a minimisation method, it proved expedient to smooth the experimental data by integrating the spectrum over a frequency range. Figure 5 shows that the data is clearly segregated into different particle size categories and is also ranked in the correct order. As predicted by the analysis of the previous section, it also shows a drift towards a lower frequency as the particle size is increased. The model spectrum given be Equation (25) was also smoothed using the same integration technique, and Figure 5 shows how the model signature changes as the particle size is increased. It can be seen that the model predictions span the experimental data and that a minimisation method (whereby the Euclidean distance between the experimental data and the model output is minimised) should be able to automate the inverse problem of recovering the particle size. To quantify the difference between the experimental data

and the model output, the following expression is utilised

$$p(b) = \sum_{i=1}^{N} (\hat{E}(\omega_i) - M(\omega_i, b))^2, \tag{31}$$

where $\hat{E}$ is the integrated experimental frequency response, M is the integrated theoretical model frequency response and b is the particle size. Figure 5 shows that minima for each of the different particle size categories are obtained and are ranked in the correct order (see Table 3). Considering the simplicity of this initial model, the results are extremely encouraging and compare well with the experiment.

4 Inverse Problem II: Recovery of the particle size from multi-particle experiments

The second set of data from a stirred reactor vessel containing itaconic acid particles suspended in toluene was then utilised [4]. The itaconic acid reacts with the toluene and, as it does so, the size of the itaconic acid particles reduces. The resultant shift in the impact vibration spectrum over time can then be used to non-invasively recover the particle size and hence monitor the reaction process. These particular materials were chosen as the reaction is a relatively simple one, the materials are readily available and the itaconic acid particles can be easily sieved to give desired particle size ranges. Although this experimental work successfully recovered the particle size by monitoring the frequency shift in the spectrum as the particle size reduced, it was clear that a mathematical model of the underlying physics was required to clarify the role of the different system parameters in the spectral response and its sensitivity to changes in these parameters [4].

4.1 Particle movement prior to impact

A simple model of the particle movement in the vessel is derived which restricts the balance of forces on the particle to the radial direction only, with the centrifugal force being balanced by particle drag and a boundary layer effect near the wall surface. This compo-

nent of the model provides the velocity of impact needed for the subsequent vibrational analysis. By considering a spherical particle falling due to gravity in a viscous fluid, the particle weight is approximately equal to its drag force so that the approximate particle mass is given as ([21], p251)

$$m = \frac{4\pi}{3} b^3 (\rho_b - \rho_f), \tag{32}$$

where ρ_b and ρ_f are the densities of the particle and fluid respectively and b is the particle radius. Incorporating the centrifugal force effect and letting $x = x(t)$ be the distance of the particle from the centre of the container then gives ([21], p406)

$$m\frac{\partial^2 x}{\partial t^2} = mw^2 x - 6\pi b\mu \frac{\partial x}{\partial t}, \tag{33}$$

where w is the stirrer rotation speed and μ is the viscosity of the fluid. Since Equations (32) and (33) are defined for an infinite vessel, a correction term must be incorporated to account for the near wall boundary and finite extent of the fluid ([21], p255). The drag force, F_D, is rewritten

$$F_D = 6\pi b\mu \left(1 + \frac{2\gamma b}{R - x}\right) \frac{\partial x}{\partial t}, \tag{34}$$

with γ denoting a geometrical constant (given as 2.104 for a circular cylinder,[21], p156), and R is the vessel radius. Equation (33) can now be re-written as

$$\frac{\partial^2 x}{\partial t^2} = w^2 x - \frac{9\mu}{2b^2(\rho_b - \rho_f)} \left(1 + \frac{2\gamma b}{R - x}\right) \frac{\partial x}{\partial t}. \tag{35}$$

In order to approximate the particle impact velocity u_0, assume that the particle acceleration is initially zero and that the boundary layer thickness is ϵ, where $\epsilon \ll 1$, so that the distance from the boundary to the vessel centre can be written as $x = R - \epsilon$. Then

$$u_0 = \frac{2b^2 w^2 (R - \epsilon)(\rho_b - \rho_f)}{9\mu(1 + 2\gamma b/\epsilon)}. \tag{36}$$

4.2 Multi-particle experiments

A series of multi-particle experiments have been performed for a 1 litre glass bell-shaped vessel with a glass stirrer rod and paddle, attached to a motor (see Figure 5) [4]. Itaconic acid was stirred in toluene with three specific size categories: less than 251 μm, between

251 μm and 500 μm and between 500 μm and 850 μm. The signals from the particle-wall collisions were then collected using a Nano 30 piezoelectric transducer [20] directly adhered to the side of the vessel. Full details of the experiment have been published elsewhere [4]. The transducer position and attachment, the fill level, the stir rate (impact velocity), concentration and temperature were varied. It was found that the particle size noticeably affected the vibration spectrum but it was far less sensitive to changes in the stir rate. The particles in the fluid, impact the vessel wall at random locations, some of which can be relatively far from the transducer position. Nevertheless, the experimental data indicate that the frequency of the peak response is less sensitive to these variations than to the particle size. This may be due to the attenuation of the vibrations arising from particles impacting far from the transducer location and from the spatial averaging effects of the particles impacting in all directions surrounding the transducer position. Figure 5 shows the multi-particle acoustic emission spectra from these experiments. Although the signature of each data set is dominated by the transducer characteristics, this figure agrees with the theoretical prediction that the main lobe shifts to a lower frequency as the particle size is increased. By smoothing this data set, the frequency of the main lobe can be extracted and plotted as a function of the particle size (see Figure 5). The model shows reasonable agreement with the experimental dependency on particle size b. Most importantly, both curves show the frequency of the peak response monotonically decreasing as the particle size increases. Integrating the data shown in Figure 5 shows that each of the three particle size categories are segregated and correctly ranked (see Figure 5). The model results span the experimental data across a similar range of particle sizes and consequently calculating the difference between the two sets of data using Equation (31) shows that the minima in $p(b)$ appear correctly ranked according to their particle size categories (see Figure 5 and Table 4). Table 4 shows that the recovered particle size is less accurate for the larger particle sizes. This may be due to the model assumptions made, or to the experimental data being dominated by the transducer response. The single-particle and the multi-particle experiments both agree with the theoretical prediction that the main spectral lobe shifts to a lower frequency as the particle size increases. In

addition, a quantitative comparison between the forward model and the experimental data has facilitated an automated particle size recovery method.

5 Conclusion

The use of ultrasonics as a process measurement technique has many advantages which are due in part to it being non-invasive and relatively inexpensive. In batch reactors, containing a particle laden fluid, the recovery of the particle size could be used to monitor the reaction process. Previous experimental and numerical simulations have used the vibrations emitted from the particles impacting with a plate, and they have shown that the frequency of the peak pressure was inversely proportional to the particle size. This paper analysed a mathematical model of this particle-plate interaction to explicitly show this dependency. Here we examined a simpler, and more controlled, experimental set-up; the impact of a spherical particle with a thin circular plate. Using a set of approximations based on series expansions, the explicit dependency of the peak pressure frequency (ω_{max}) on the system parameters was derived. It was found that (ω_{max}) is inversely proportional to the particle size and the particle density, and directly proportional to the particle impact velocity (or the height that the particle is dropped from). The sensitivity to these parameter changes can also be gauged and it was shown that the dominant factor in these frequency shifts in the spectrum is due to changes in the particle size.

To validate this approach an experiment involving spherical particles being dropped onto a circular plate was utilised. In contrast to previous work the vibration response of the plate was measured using an ultrasonic transducer in contact with the plate. The experiments showed that (ω_{max}) does decrease as the particle size increases, in agreement with the model predictions. The paper then proposed an inverse methodology to automatically recover the particle size. In the first instance the data from the single particle experiments was used. There was good agreement between the model output and the experimental data and the inverse methodology was able to successfully recover the particle size. Encouraged by these results, some multi-particle experimental data was then used to recover the particle size in this setting. Even though the forward model neglected

many of the additional complexities of these experiments the inverse methodology was still successful. This paper has therefore theoretically derived for the first time the explicit dependency of the frequency of the peak vibration response on the system parameters and, from the knowledge gained, has developed a method for automating the recovery of the particle size from impact vibration spectra obtained using an ultrasonic transducer. The next stage will be to derive an analytic expression for the magnitude of the impact frequency response (F_0) so that the particle concentration, in the multi-particle setting, can be recovered.

Acknowledgments

The authors would like to thank EPSRC for their funding support (GR/P03209/01) and the Royal Society for the award of a University Research Fellowship to AN.

References

[1] M.J.W.Povey, T.J.Mason, *Ultrasound in food processing*, Blackie Academic and Professional, London, UK, 1998.

[2] P.Troccaz, R.Woodcock, F.Laville, Acoustic radiation due to the inelastic impact of a sphere on a rectangular plate. *J. Acoust. Soc. Am.* 108(5) Pt.1 (2000) 2197-2202.

[3] D.J.Buttle, C.B.Scruby, Characterization of particle impact by quantitative acoustic emission. *WEAR* 137 (1990) 63-90.

[4] A.Nordon, Y.Carella, A.Gachagan, D.Littlejohn, G.Hayward, Factors affecting broadband acoustic emission measurements of a heterogeneous reaction. *Analyst* 131 (2006) 323-330.

[5] D.Takahashi, Frequency analysis of sound radiation from an impact-excited plate. *J. Acoust. Soc. Am.* 19(5) (1992) 2708-2713.

[6] J.Hidaka, A.Simosaka, H.Ito, S.Miwa, Instantaneous measurement of particle size and flow rate by the parameters of impact sound between particles and a circular plate. *KONA* 10 (1992) 175-183.

[7] A.Akay, M.Latcha, Sound radiation from an impact-excited clamped circular plate in an infinite baffle. *J. Acoust. Soc. Am.* 74(2) (1983) 640-648.

[8] J.R.W.Boyd, J.Varley, The uses of passive measurement of acoustic emissions from chemical engineering processes. *Chemical Engineering Science* 56 (2001) 1749-1767.

[9] G.P.Hancke, R.Malan, A modal analysis technique for the on-line particle size measurement of pneumatically conveyed pulverized coal. *IEEE Transactions on Instrumentation and Measurement* 47(1) (1998) 114-122.

[10] P.L.Lee, R.B.Newell, I.T.Cameron, *Process control and management,* Blackie Academic and Professional, London, UK, 1998.

[11] M.F.Leach, G.A.Rubin, J.C.Williams, Particle size determination from acoustic emissions. *Powder Tech.* 16 (1977) 153-158.

[12] J.Hidaka, A.Shimosaka, S.Miwa, The effects of particle properties on the parameters of impact sound between two particles. *KONA* 7 (1989) 4-14.

[13] J.Hidaka, A.Shimosaka, Parameters of radiated sound and state variables in flowing particles. *Intl. J. Mod. Phys. B* 7 (1993) 1965-1975.

[14] P.D.Thorne, D.J.Foden, Generation of underwater sound by colliding spheres. *J. Acoust. Soc. Am.* 84 (6) (1998) 2144-2152.

[15] P.D.Thorne, The measurements of acoustic noise generated by moving artificial sediments. *J. Acoust. Soc. Am.* 78(3) (1985) 1013-1023.

[16] P.D.Thorne, Laboratory and marine measurements on the acoustic detection of sediment transport. *J. Acoust. Soc. Am.* 80(3) (1986) 899-910.

[17] A.Akay, M.Tokunaga, M.Latcha, A theoretical analysis of transient sound radiation from a clamped circular plate. *J. App. Mech.* 54 (1984) 41-47.

[18] W.Goldsmith, *Impact:the theory and physical behaviour of colliding solids*, Edward Arnold Publishers Ltd., London, UK, 1960.

[19] N.Townshend, Monitoring of particulate processes using acoustic emission, MSci Project Thesis, University of Strathclyde, Department of Pure and Applied Chemistry, 2006.

[20] Physical Acoustics Limited, Cambridge, UK.

[21] T.Allen, *Particle size measurement*, Chapman and Hall, London, UK, 1990.

[22] www.camglassblowing.co.uk/gproperties.htm (Accessed 20 May 2007).

[23] www.chemexper.com (Accessed 20 May 2007).

[24] www.npl.co.uk/mass/guidance/buoycornote.pdf (Accessed 20 May 2007).

[25] A.Nordon, R.J.H.Wadell, L.J.Bellamy, A.Gachagan, D.McNab, D.Littlejohn, G.Hayward, Monitoring of a heterogeneous reaction by acoustic emission, Document 04/T1/2, CPACT, University of Strathclyde, Glasgow, UK, 2004.

[26] www.engineersedge.com/fluid flow/fluid data.htm (Accessed 20 May 2007).

Figure 1: Time domain plate displacement for a glass particle dropped onto a glass plate highlighting the branch split point $\frac{\pi}{\omega_0}$ (see Equation (1)). Refer to Table 1 and Table 2 for typical parameter values.

Figure 2: (a) Theoretical plate acceleration calculated from an FFT of the second branch of Equation (1) (——) and the corresponding approximate acceleration calculated from Equation (23) (- - -). (b) Moving average (with 100 points) of the data presented in plot (a). Table 1 and Table 2 contain typical parameter values.

Figure 3: Variation of P_1 with the damping coefficient η given by Equation (28). Table 1 and Table 2 contain typical parameter values.

Figure 4: The scaled plate vibration spectrum plotted for various particle sizes (μm) using the theoretical approximation Equation (25) for a glass particle dropped onto a glass plate. Table 1 and Table 2 contain typical parameter values.

Figure 5: Comparison of the model spectra obtained from Equation (25) and the normalised spectra arising from the single particle experiments. Three different experimental particle sizes (μm) are depicted. Table 1 and Table 2 contain typical parameter values.

Figure 6: Difference between the model spectrum (see Equation (25)) and the experimental spectrum for various particle sizes (μm). Table 1 and Table 2 contain typical parameter values.

Figure 7: The schematic of the model set-up.

Figure 8: The multi-particle experimental set-up for Itaconic Acid stirred in Toluene. Table 1 and Table 2 contain typical parameter values.

Figure 9: The plate vibration spectra arising from Itaconic acid in Toluene experiments. Three different particle size ranges (in μm) are shown. Table 1 and Table 2 contain typical parameter values.

Figure 10: The theoretical prediction of ω_{max} (Equation (29)) for the main maxima frequency (- - -) as a function of the particle size, for Itaconic acid in Toluene and the corresponding experimental data (——). Table 1 and Table 2 contain typical parameter values.

Figure 11: Comparison of the theoretical model obtained by Equation (25) and the integrated spectra arising from the multi-particle experiments with Itaconic Acid in Toluene. Three experimental particle size ranges (in μm) are shown. The numbers in the legend refer to the particle's radius in μm. Table 1 and Table 2 contain typical parameter values.

Figure 12: Difference between the theoretical model spectrum and the experimental spectrum for various particle size ranges using Equation (31) (in μm). Table 1 and Table 2 contain typical parameter values.

Table 1: Parameter values.

Table 2: Material Properties: a : [22], b : [23], c : [24], d : [25], e : [26].

Table 3: Experimentally measured single particle size ranges compared with their calculated values obtained by minimising Equation (31).

Table 4: Experimentally measured multi-particle size ranges compared with their calculated values obtained by minimising Equation (31).

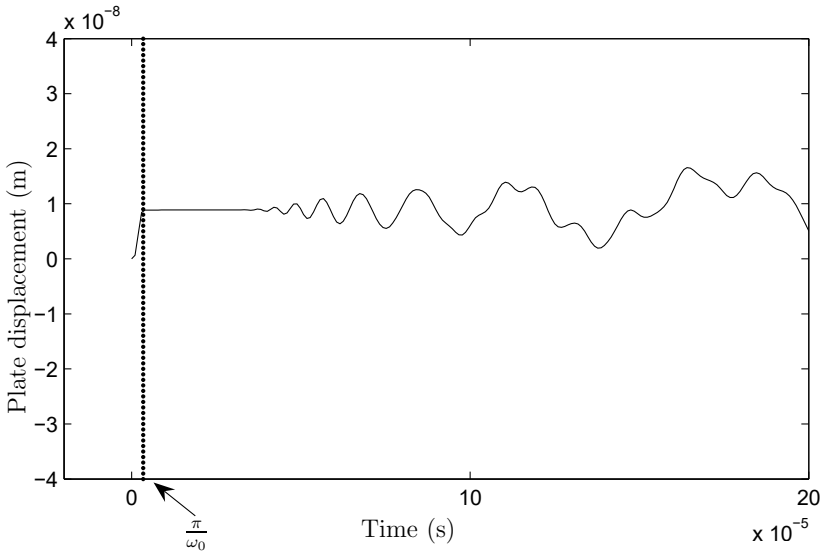
x 10^−8
Plate displacement (m)
Time (s)
x 10^−5
π/ω0

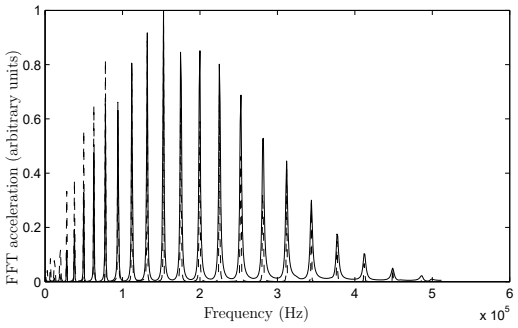
FFT acceleration (arbitrary units)
Frequency (Hz)
x 10^5

(a)

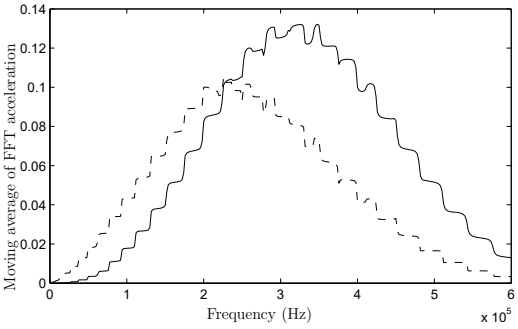
Moving average of FFT acceleration
Frequency (Hz)
x 10^5

(b)

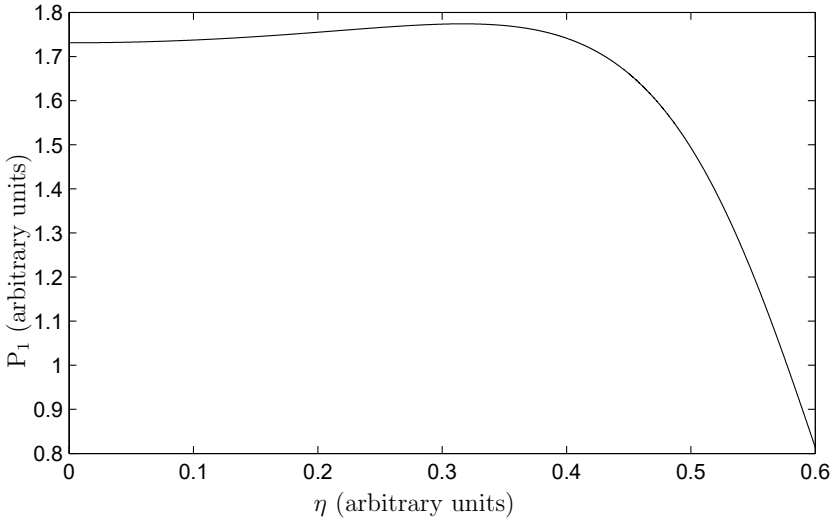
P1 (arbitrary units)
η (arbitrary units)

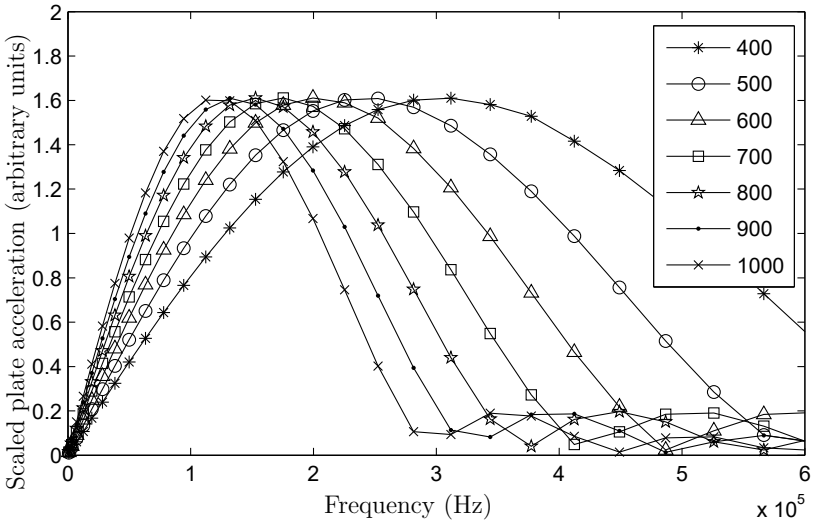
Scaled plate acceleration (arbitrary units)
Frequency (Hz)
x 10^5
400
500
600
700
800
900
1000

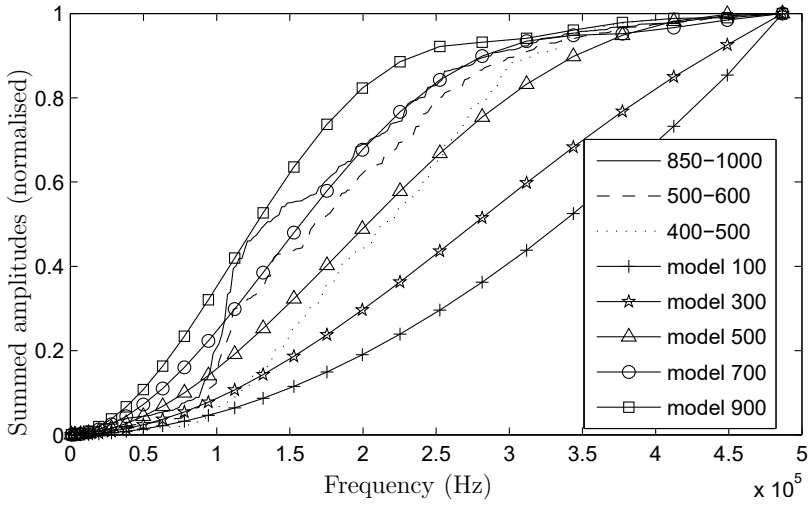
Summed amplitudes (normalised)
Frequency (Hz)
x 10^5
850−1000
500−600
400−500
model 100
model 300
model 500
model 700
model 900

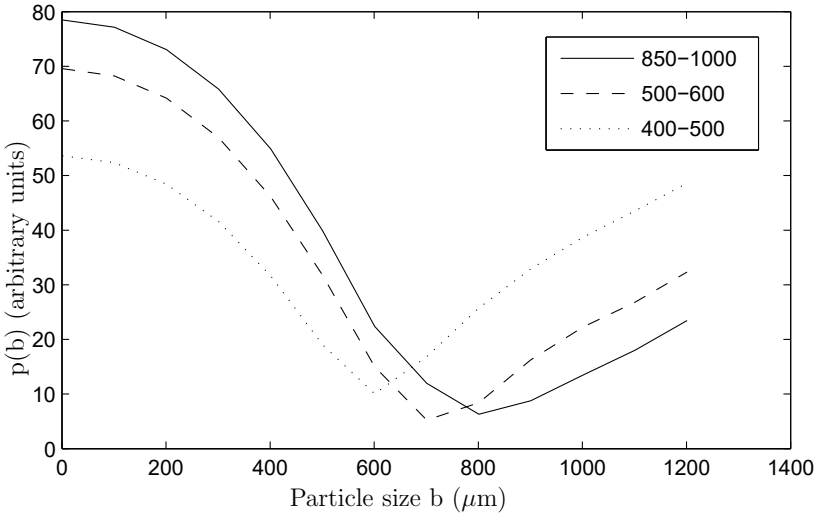
p(b) (arbitrary units)
Particle size b (μm)
850−1000
500−600
400−500

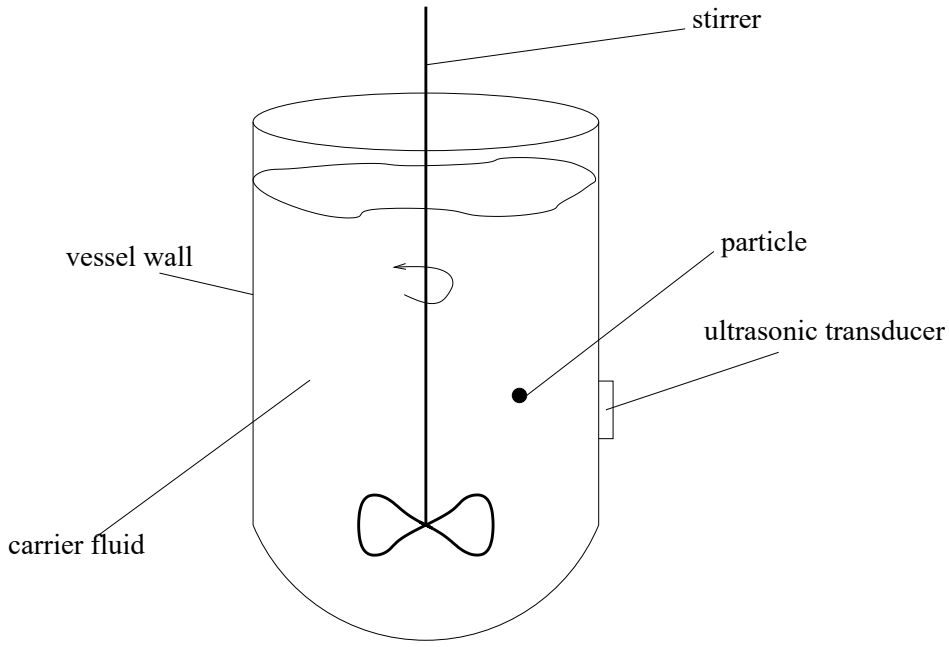
stirrer
vessel wall
particle
ultrasonic transducer
carrier fluid

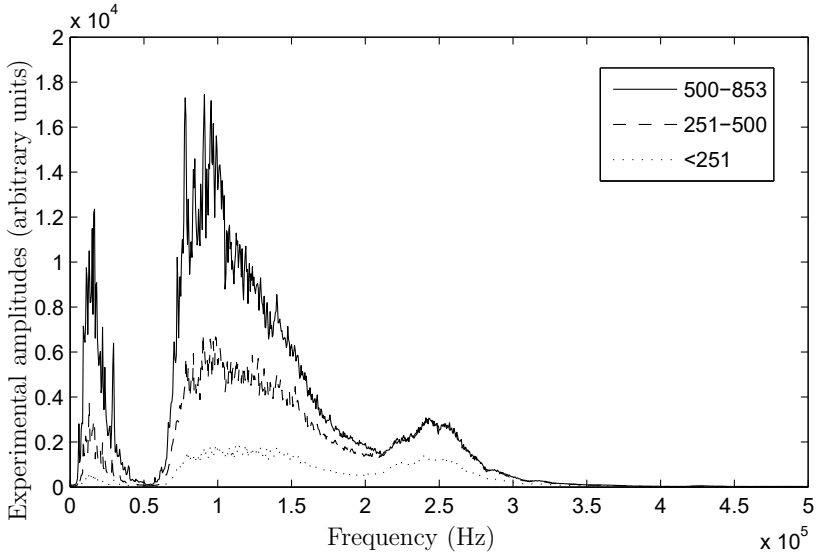
x 10^4
Experimental amplitudes (arbitrary units)
Frequency (Hz)
x 10^5
500−853
251−500
<251

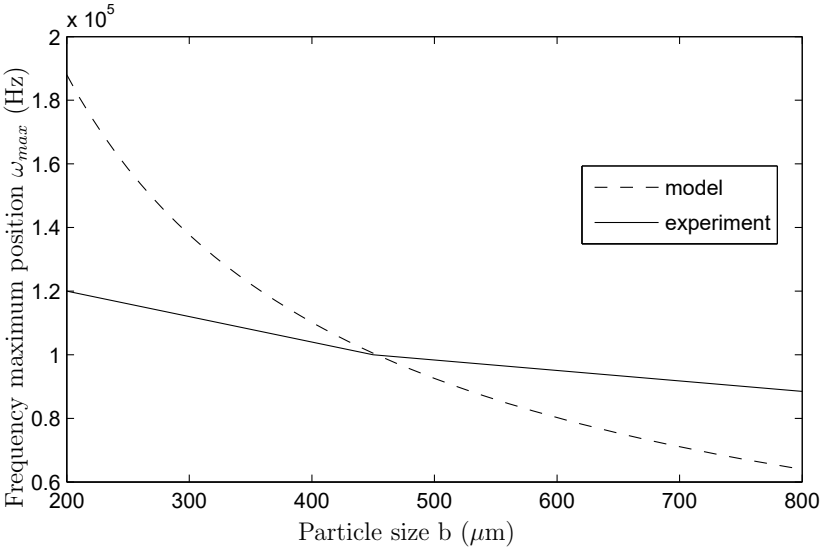
x 10^5
Frequency maximum position ω_{max} (Hz)
Particle size b (μm)
model
experiment

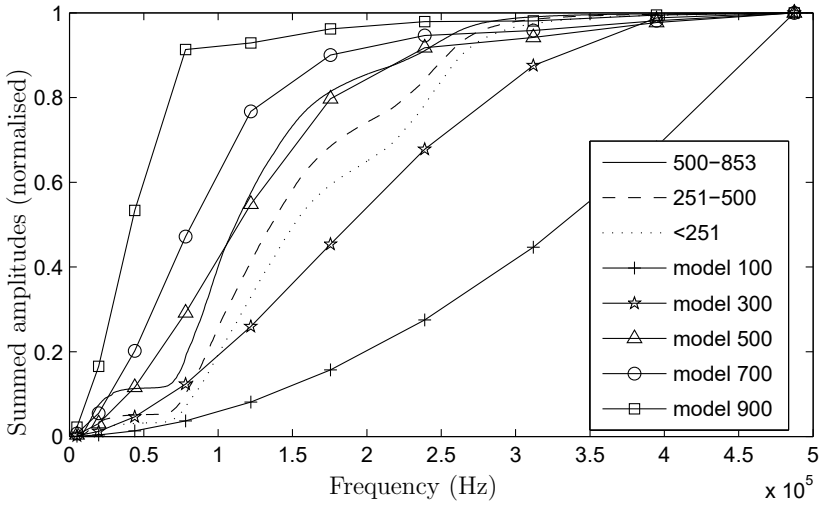
Summed amplitudes (normalised)
Frequency (Hz)
x 10^5
500−853
251−500
<251
model 100
model 300
model 500
model 700
model 900

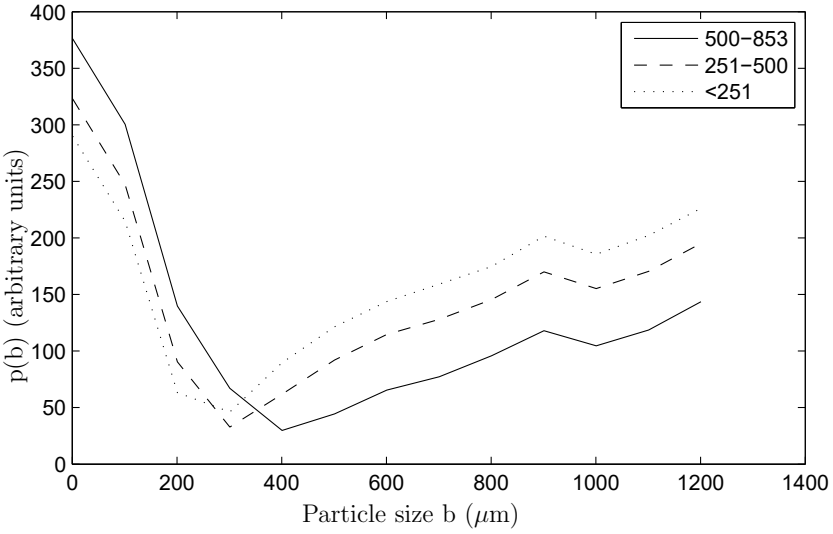
500−853
251−500
<251
p(b) (arbitrary units)
Particle size b (μm)
0
50
100
150
200
250
300
350
400
0
200
400
600
800
1000
1200
1400

Table 1:

Parameter	Symbol	Value
Particle radius	b	500μm
Plate radius	a	0.1m
Plate thickness	h	0.01m
Particle impact point	r	0.001m
Vessel radius	R	0.1m
Damping coefficient	η	0.01
Stir rate	ω	125rpm

Table 2:

	units	Glass	Itaconic Acid	Air	Toluene
Density ρ	$\mathrm{kg\,m^{-3}}$	2230^{a}	1573^{b}	1.2^{c}	865^{b}
Poisson's Ratio ν	-	0.21^{a}	0.5^{d}	-	-
Young's Modulus E	$\mathrm{N\,m^{-2}}$	$6.3 \times 10^{9\,a}$	$1 \times 10^{9\,d}$	-	-
Viscosity μ	$\mathrm{kg\,m^{-1}\,s^{-1}}$	-	-	-	$6.8 \times 10^{-3\,e}$

Table 3:

Actual size (μm)	Approx. Recovered Size (μm)
$850 - 1000$	800
$500 - 600$	700
$400 - 500$	600

Table 4:

Actual size (μm)	Approx. Recovered Size (μm)
$500 - 853$	400
$251 - 500$	290
< 251	220